Expectations for the Deep Impact collision from modelling of cometary nuclei.

O. Mousis, Ulysse Marboeuf, Jean-Marc C. Petit, J. Klinger

Mon. Not. R. Astron. Soc. **362,** L40–L44 (2005) doi:10.1111/j.1745-3933.2005.00070.x

Expectations for the *Deep Impact* collision from modelling of cometary nuclei

O. Mousis,[1⋆] U. Marboeuf,[1] J.-M. Petit[1] and J. Klinger[2]

[1] *Observatoire de Besançon, CNRS-UMR 6091, BP 1615, 25010 Besançon Cedex, France*
[2] *Tizin, 38210 Tullins, France*

Accepted 2005 June 25. Received 2005 June 15; in original form 2005 June 1

ABSTRACT

Using the cometary nucleus model developed by Espinasse et al., we calculate the thermodynamical evolution of Comet 9P/Tempel 1 over a period of 360 yr. Starting from an initially amorphous cometary nucleus which incorporates an icy mixture of H_2O and CO, we show that, at the time of *Deep Impact* collision, the crater is expected to form at depths where ice is in its crystalline form. Hence the subsurface exposed to space should not be primordial. We also attempt an order-of-magnitude estimate of the heating and material ablation effects on the crater activity caused by the 370-kg projectile released by the *Deep Impact* spacecraft. We thus show that heating effects play no role in the evolution of crater activity. We calculate that the CO production rate from the impacted region should be about 300–400 times higher from the crater resulting from the impact with a 35-m ablation than over the unperturbed nucleus in the immediate post-impact period. We also show that the H_2O production rate is decreased by several orders of magnitude at the crater base just after ablation.

Key words: comets: individual: 9P/Tempel 1.

1 INTRODUCTION

On 2005 July 4, the 370-kg projectile released by the dual *Deep Impact* (*DI*) spacecraft will collide with the short-period Comet 9P/Tempel 1 one day before perihelion at a velocity of 10.2 km s^{-1}. At the same time, the flyby spacecraft will take optical images and near-infrared spectra of the nucleus, the crater formation process, the resultant crater and ejecta, and any induced outgassing. The main scientific goals of this mission are to infer the bulk properties of the cometary nucleus, understand better its internal structure, compare outgassing composition before and after impact, and derive some constraints on the crater formation process.

In the present work, we use the cometary nucleus model developed by Espinasse et al. (1991) to examine the plausible current thermodynamical state of Comet 9P/Tempel 1. Starting with an initially amorphous cometary nucleus, we follow the evolution of the stratigraphy of Comet 9P/Tempel 1 over a period covering the last 360 yr of its orbital history.[1] This allows us to infer the nature of the ice, which may be amorphous (therefore pristine) or crystalline, according to the thermal evolution of the nucleus, and which should be revealed at the crater base after the impact from the *DI* projectile. We also give an order-of-magnitude estimate of the combined effects of the material ablation and heating on the crater activity caused by the *DI* impactor. Ablation consists, at the time of the impact, of the removal of an outer icy layer of the nucleus, the thickness of which corresponds approximately to the crater depth. Impact heat is transferred to the crater subsurface immediately after ablation, and its propagation occurs in the radial direction of the cometary nucleus, following the approach described by Orosei et al. (2001). Once these two processes are taken into account, this enables us to calculate the production rates of the main volatiles (H_2O and CO) that are expected to outgas from the crater.

In Section 2, a brief description of the nucleus model is presented. We also give some details concerning the impact modelling and the choice of nucleus parameters. In Section 3, we calculate the thermodynamical evolution of Comet 9P/Tempel 1 over the last 360 yr of its orbital history. We also estimate in this section the effects induced by impact heating and ablation on the crater activity. Section 4 is devoted to conclusions.

2 MODELS

2.1 The cometary nucleus model

The nucleus model employed in this work is the 1D model originally developed by Espinasse et al. (1991). This model takes a sphere (initially homogenous) composed of a highly porous predefined mixture of water ice (the dominant constituent) and CO ice in specified proportions. We consider that the mixture is initially amorphous because of the dynamical evolution of the comet

⋆E-mail: Olivier.Mousis@obs-besancon.fr

[1] The orbital evolution of this comet is poorly constrained at earlier epochs (see Section 2.3).

described in Section 2.3. CO is trapped in the amorphous water ice, with the remaining CO, if any, being condensed in the pores. When heated, the condensed CO sublimates first, then the trapped CO is released during the transition from amorphous to crystalline water ice. The model is based on the simultaneous resolution for the whole nucleus of a heat diffusion equation and an equation of gas diffusion in the pore system. It accounts for heat transmission, gas diffusion, and sublimation/condensation of volatiles within the matrix, solving the partial differential equations that describe the nucleus. However, note that the model used here has been the subject of several refinements in recent years (Espinasse et al. 1993; Orosei et al. 1995, 1999). In particular, with the incorporation of dust and the use of more appropriate numerical methods, the recent versions of the model provide an improved description of the interior evolution of the nucleus. On the other hand, the present work started a few months ago using the original nucleus model of Espinasse et al. (1991). In these conditions, the imminence of the *DI* event did not allow us to take time to incorporate these latter improvements in our code. Nevertheless, even in its current version, this model allows us to examine some interesting clues concerning the thermochemical state of Comet 9P/Tempel 1, both before and after the collision.

2.2 Impact modelling

In this work, the collision between the *DI* projectile and Comet 9P/Tempel 1 is characterized in terms of (1) the ablation of cometary material due to the cratering event, and (2) the amount of kinetic energy delivered in the form of heat to the target by the impactor itself. Ablation consists of the removal, at the time of the impact, of an outer icy layer of the cometary nucleus, the thickness of which corresponds roughly to the crater depth due to the projectile impact. Immediately after ablation, impact heat is transferred to the crater base and its propagation in the cometary nucleus is described following the approach of Orosei et al. (2001). Because of the 1D nature of the model, lateral heat diffusion is neglected. As pointed out by Orosei et al. (2001), this method has some limitations. In particular, the depth at which the impact can thermally alter the comet must be considered as an upper limit. In the present case, the distribution of impact heat results in a homogeneous energy density deposited in the crater subsurface within a cylinder the cross-section and depth of which correspond respectively to the crater diameter and the size of the projectile. Once these two physical processes are taken into account in our model, it is possible to give an order-of-magnitude estimate of the combined effects of the material ablation and heating on the crater activity caused by the *DI* projectile.

2.3 Choice of parameters

Table 1 summarizes the set of parameters selected for the nucleus of Comet 9P/Tempel 1. Two different CO:H_2O initial ratios were selected for the composition of the comet, namely 5 per cent for the first model ('CO-poor comet'), and 15 per cent for the second model ('CO-rich comet'). In the model, any CO in excess of 10 per cent appears as condensed CO ice. The resulting densities, which have been determined using a porosity of 0.7, are compatible with the estimated density of Comet 9P/Tempel 1 (Belton et al. 2005). The nucleus radius and geometric albedo are taken from Lamy et al. (2004) and Lisse et al. (2005a) respectively. The initial pore radius has been fixed to 10^{-5} m, following De Sanctis et al. (1999). Emissivity ϵ has been chosen to be close to 1 since the nucleus can be modelled as a blackbody because of the high porosity of its material. The initial temperature of 30 K for the whole nucleus corresponds to the equilibrium temperature for a highly conducting black sphere orbiting at about 90 au from the Sun. Following Coradini et al. (1997), we have used the formula of Russel (1935) to compute the bulk conductivity from those of amorphous and crystalline water ice (Klinger 1980).

Table 1. Initial parameters of nucleus model.

Parameter	CO-poor comet	CO-rich comet
Structural		
Radius (R)	3.1 km	
Bulk density (ρ)	283 kg m^{-3}	296 kg m^{-3}
Porosity (p)	0.7	
Pore radius (r_0)	10 μm	
Material		
Fraction of trapped CO	0.05	0.15
Albedo (A)	0.04	
Emissitivity (ϵ)	0.95	
Temperature	30 K	

Table 2. Orbital parameters (semi-major axis a, eccentricity e) for the last 360 yr. Epochs refer to the beginning of each orbit.

	a (au)	e	Epochs		a (au)	e	Epochs
Orbit 1	3.92	0.27	1645	Orbit 6	3.29	0.46	1870
Orbit 2	3.71	0.32	1668	Orbit 7	3.48	0.4	1882
Orbit 3	3.42	0.43	1704	Orbit 8	3.24	0.47	1941
Orbit 4	3.21	0.45	1776	Orbit 9	3.12	0.52	1954
Orbit 5	3.18	0.5	1787				

Table 2 describes the orbital history of Comet 9P/Tempel 1 over the last 360 yr. The parameters given here are averages of the orbital data from the numerical simulations reported on the NASA web site.[2] Owing to the limitations of these simulations, the orbital history of Comet 9P/Tempel 1 is poorly determined at epochs earlier than ∼1640. Hence we have opted to perform our calculations of its thermodynamical evolution during the period covered by Table 2. In this work, following papers published on the origin of short-period comets, we assume that Comet 9P/Tempel 1 originates from the Kuiper Belt region [see Morbidelli (1999) for a review]. Since the Kuiper Belt was probably rather cold at the epoch of formation of the solar nebula, this comet must have formed from pristine ices directly originating from the pre-solar cloud, as predicted by Mousis et al. (2000), thus justifying the assumption of an initially amorphous nucleus.

Since the amount of energy transported by the projectile is quite small ($E_{\rm kinetics} = 1.9 \times 10^{10}$ J, with a projectile mass of 370 kg and velocity of 10.2 km s^{-1}), we have deliberately adopted a set of impact parameters that optimize the influence of collisional heating on the thermodynamical behaviour of the nucleus. Adopted values of 50 m for the crater size and 35 m for its depth derive from the cratering scenarios established by Schultz & Anderson (2005) for the *DI* collision, and have been chosen to favour a higher energy density and a deeper energy deposition. We have also optimized the energy transfer due to the impact by assuming that 90 per cent of the kinetic energy of the projectile is deposited as heat in the nucleus, with the remaining 10 per cent being distributed into the ejected fragments.

[2] http://deepimpact.jpl.nasa.gov/science/tempel1-orbitalhist.html

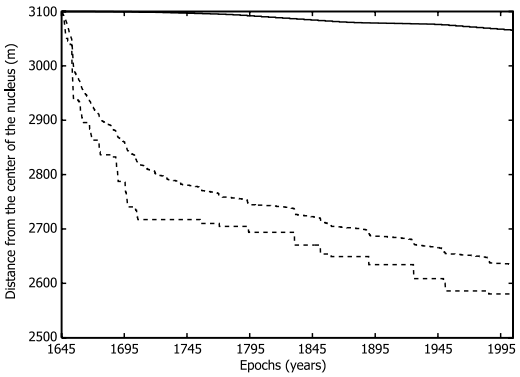

Figure 1. Evolution of the stratigraphy of the CO-poor comet over the last 360 yr, assuming an initially amorphous nucleus. The lines represent, from top to bottom, the surface, the lower limit of the complete crystalline layer and the upper limit of the totally amorphous ice layer as a function of orbital evolution. The lower limit of total depletion of the trapped CO is the same as the lower limit of the complete crystalline layer.

3 RESULTS

3.1 Thermodynamical evolution of Comet 9P/Tempel 1

Fig. 1 shows a plausible thermodynamical evolution of the nucleus of a CO-poor comet over a period covering the last 360 yr in the orbit of Comet 9P/Tempel 1. Starting with an initially amorphous nucleus, the amorphous/crystalline phase transition takes place at the same time as CO emission starts. This phase transition occurs deeper as soon as the comet is injected into an orbit closer to the Sun. At the end of the 360-yr period, the surface ablation reaches a depth of 34 m and the lower limit of the complete crystalline layer is located 427.8 m below the surface. An intermediary layer containing a mixture of both amorphous and crystalline H_2O ice, and solid CO (trapped in the amorphous matrix or condensed in the pores), is formed between the crystalline layer and the undifferentiated core. The upper limit of the totally amorphous layer is located 485 m below the surface.

Fig. 2 is similar to Fig. 1 but instead examines a CO-rich comet. At the end of the calculations, the surface ablation reaches a depth of 37.4 m and the lower limit of the complete crystalline layer is located 201 m below the surface. The upper limit of the undifferentiated core is located at a depth of 215 m. In that case, the crystalline layer is much thinner than in the CO-poor comet case. As stated by Espinasse et al. (1991), the presence of a larger amount of CO in the nucleus tends to slow the propagation of the amorphous-to-crystalline phase transition because a large fraction of the incoming energy is used to vaporize the extra CO. We have performed the same calculations as in Figs 1 and 2 but for porosities of 0.3. Adopting a lower porosity tends to increase the amplitude of crystallization. Indeed, the lower limit of the crystalline layer is found to be deeper (555.9 m for the CO-poor comet and 236.2 m for the CO-rich comet), even if, in both cases, the value of the surface ablation depth after 360 yr of orbital evolution is lower (12.9 m for the CO-poor comet and 14.2 m for the CO-rich comet).

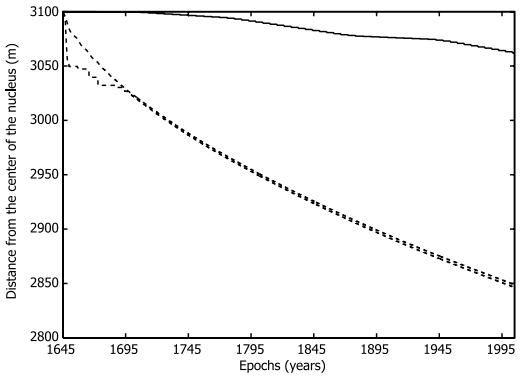

Figure 2. As in Fig. 1 but for the case of the CO-rich comet.

The calculations presented here suggest that, even if the orbital history of Comet 9P/Tempel 1 is not taken into account at epochs prior to the last 360 yr, the thickness of the crystalline layer exceeds greatly the depth of the crater expected to be formed by the *DI* projectile. This suggests that the nucleus material revealed at the crater base should not be primordial. A phase transition between amorphous and crystalline H_2O ice has occurred over a minimum of several hundred metres depth from the surface of the nucleus during the thermal history of the comet, and the abundance of CO present in this layer no longer reflects its primordial value at the time of comet formation.

Fig. 3 shows the H_2O and CO production rates [$Q(H_2O)$ and Q(CO) respectively] for both CO-rich and CO-poor comets. It can be seen that the production rates at perihelion vary as a function of the orbital history of Comet 9P/Tempel 1. Production rates at the beginning of the simulation are meaningless, as they result from the abrupt injection from a distant orbit into an orbit close to the Sun. After about 3 orbits, thermal equilibrium is reached and production rates are informative. The H_2O production rates of both CO-rich and CO-poor comets are practically identical. On its current orbit, the H_2O production rate given by the two models is $\sim 1.5 \times 10^{-3}$ mole m^{-2} s^{-1} at perihelion, i.e. $\sim 1.1 \times 10^{29}$ molecule s^{-1} for the whole nucleus. This latter value is around 5 times higher than the gas production rate derived from measurements of the activity of Comet 9P/Tempel 1 made by A'Hearn et al. (1995). Such a difference can easily be explained by considering that the activity is concentrated on the subsolar point (Enzian et al. 1999). Additionally, dust accumulation on the surface may also modulate the activity (De Sanctis et al. 1999). This latter possibility is confirmed by the recent work of Lisse et al. (2005b) who derived, using a thermal model, that about 9 ± 2 per cent of the surface of Comet 9P/Tempel 1 is active at perihelion.

As shown in Fig. 3, the evolution of the CO production rate varies as a function of the initial CO:H_2O ratio adopted in the nucleus. At the very beginning, the peaks in the production rates are more

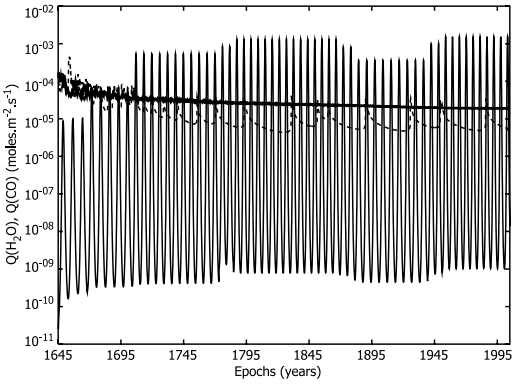

Figure 3. Production rates over the last 360 yr. The graphs represent $Q(H_2O)$ for both models (solid line), and Q(CO) for the CO-rich comet (bold solid line) and for the CO-poor comet (dashed line).

important in the CO-rich comet than in the CO-poor comet. With time, the increasing thickness of the crystalline layer tends to lower the Q(CO) of the CO-poor comet. The quasi-constant CO production rate in the case of the CO-rich comet results from the regular sublimation of the portion of CO condensed in the pores. For the CO-poor comet, peaks in Q(CO) are strongly correlated with peaks of crystallization (the steep slope in the lower limit of the crystalline zone in Fig. 1), which in turn occur slightly after the orbit has changed for a new perihelion distance. At the time of the *DI* encounter, which is about 1 d before perihelion, Q(CO) is about 5×10^{-6} and 2×10^{-5} mole m^{-2} s^{-1} in the cases of CO-poor and CO-rich comets, respectively.

The most important caveat is that strong surface erosion due to insolation before impact could drastically decrease the depth of crystalline ice. In addition, our model does not consider the latitudinal variation of the insolation.

3.2 Effects of impact heating and ablation

We have calculated the heating induced by the energy transfer to the crater base, once ablation is over. Adopting the impact parameters given in Section 2.3 which favour a higher energy density, this results in a slight temperature elevation in the crater subsurface ($\sim$ a few K), compared with the nucleus temperature at the same depth just before the collision ($\sim$140 K). As our nucleus model shows, this temperature increase is too low to ease the subsequent sublimation of the exposed H_2O ice at the crater base. Hence heating effects due to the impact play no role in the evolution of the crater activity.

However, ablation of cometary material due to the cratering leads to several important consequences. Just after ablation, and due to the delay required for the subsurface to reach an equilibrium state with insolation, the freshly exposed ice remains at a lower temperature than the average at the surface for a long time. As a result, the H_2O production rate $Q(H_2O)$ is decreased by several orders of magnitude in the crater zone just after ablation [$Q(H_2O)$ is about 10^{-5} and 10^{-6} mole m^{-2} s^{-1} for CO-rich and CO-poor comets respectively, with a 35-m ablation depth]. With time, the $Q(H_2O)$ of the crater increases, such that approximately between 12 and 24 h after the impact it is still half that calculated for both CO-rich and CO-poor unperturbed comets.

Fig. 4 describes the evolution of CO production rates Q(CO) for both CO-rich and CO-poor comets following the impact, for two different ablation depths, namely 35 m (our nominal case) and 10 m. These production rates reflect the release through the crater surface of gaseous CO (mainly present in the pores of the crystalline layer of the nucleus). CO production rates for the unperturbed CO-rich and CO-poor comets are also given for comparison. It can be seen that, just after a 35-m ablation due to the impact, Q(CO) at the crater base is enhanced by a factor of about 300–400 with respect to the value for the unperturbed nucleus in both models [1.4×10^{-3} and 8.4×10^{-3} mole m^{-2} s^{-1} for Q(CO) of CO-poor and CO-rich comets, respectively]. If a 10-m ablation is considered, Q(CO) at the crater base of both models is enhanced by a factor of $\sim$100 relative to the value for the unperturbed nucleus. Values of the production rates strongly depend on the porosity of the nucleus. For a porosity of 0.3, Q(CO) is increased by about one order of magnitude both before and after the impact. Starting with a much higher rate than $Q(H_2O)$ at the crater base just after its formation, the value of Q(CO) decreases with time and meets that of $Q(H_2O)$ about 1 h after the impact for a 35-m ablation. Moreover, Q(CO) is still twice that of the unperturbed comet $\sim$48 h after the impact.

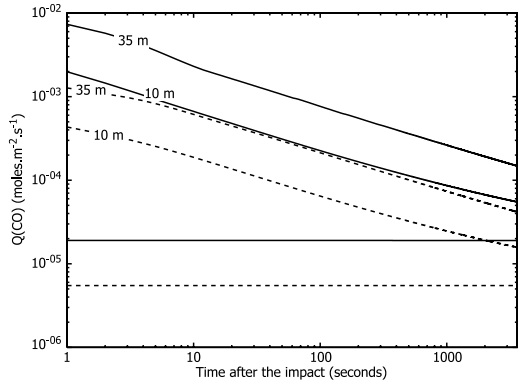

Figure 4. Evolution of Q(CO) for 1 h after the impact. Horizontal solid and dashed lines correspond to Q(CO) of the unperturbed CO-rich and CO-poor comets, respectively. From top to bottom, the oblique solid lines represent the evolution of Q(CO) of the CO-rich comet after the impact with ablations of 35 and 10 m, respectively. From top to bottom, the oblique dashed lines represent the evolution of Q(CO) of the CO-poor comet after the impact with ablations of 35 and 10 m, respectively.

4 CONCLUSIONS

Using the 1D cometary nucleus model originally developed by Espinasse et al. (1991), we have elaborated two different models, a CO-poor comet and a CO-rich comet, which could resemble Comet 9P/Tempel 1. We have calculated the thermodynamical evolution of these two models over the last 360 yr, a period during which the orbital parameters of Comet 9P/Tempel 1 are fairly well determined. Starting with an initially amorphous nucleus, we show that, at the time of impact, the thickness of the crystalline layer greatly exceeds the depth of the crater expected to be formed by the *DI* projectile. Hence the fresh ice newly exposed at the crater base should not be primordial since it has suffered a phase transition and a composition change during the thermal history of the comet.

We have also calculated the combined effects of the material ablation and heating on the crater activity caused by the *DI* projectile. Ablation consists here of the removal of an outer icy layer of the cometary nucleus at the time of the impact. Impact heat is transferred to the crater subsurface immediately after ablation as a homogeneous energy density deposited within a cylinder the cross-section and depth of which correspond to the crater diameter and the size of the projectile, respectively. As a result, because of the very limited temperature elevation ($\sim$ a few K) of the crater subsurface, we show that impact heating plays no role in the evolution of the crater activity. On the other hand, we calculate that the H_2O production rate is decreased by several orders of magnitude just after a 35-m ablation [$Q(H_2O)$ is about 10^{-5} and 10^{-6} mole m^{-2} s^{-1} for CO-rich and CO-poor comets, respectively]. For the same ablation depth, we also calculate that the CO production rate is enhanced by a factor of about 300–400 relative to the value for the unperturbed nucleus in both models in the immediate post-impact period.

Since the major effect of the impact is the ablation of the top layers, allowing a huge increase of CO production rate, these results are not sensitive to the exact impact parameters that we have used. In particular, an important decrease of deposited energy, potentially due to a lower energy transfer efficiency, would not affect our conclusions.

We are aware of the limitations of our model, this latter being based on the 'fast-rotator' approximation. However, it has been shown that it is a good assumption for the interior of the nucleus, and

also for modelling the activity of the nucleus close to the Sun (Prialnik 2002). The incorporation of dust in our calculations would have also provided a more realistic description of the thermodynamical evolution of the nucleus.

In particular, the dust trapped just beneath the nucleus surface would eventually form a dust mantle, which in turn would affect the rate of heat and gas flow at the surface (Prialnik 2002). This would also modify the local pore size distribution. On the other hand, the production rates calculated here are order-of-magnitude estimates, and predictions for the evolution of these quantities in the post-impact period are relative values. Moreover, since the thermal conductivity of dust is higher than that of amorphous ice, its presence in the nucleus would greatly ease the amorphous-to-crystalline phase transition, thus leading to a thicker crystalline layer at the termination of our calculations of the 360 yr of orbital evolution.

ACKNOWLEDGMENTS

We thank Sylvie Espinasse who made helpful suggestions about the use of her code, Jonathan Horner for valuable comments on the manuscript, and Anny-Chantal Levasseur-Regourd for profitable discussions.

REFERENCES

A'Hearn M. F., Millis R. L., Schleicher D. G., Osip D. J., Birch P. V., 1995, Icarus, 118, 223
Belton M. J. S., Meech K. J., A'Hearn M. F., Groussin O., McFadden L., Lisse C., Fernandez Y. R., Pittichova J., 2005, Space Sci. Rev., in press
Coradini A., Capaccioni F., Capria M. T., de Sanctis M. C., Espinasse S., Orosei R., Salomone M., Federico C., 1997, Icarus, 129, 317
De Sanctis M. C. et al., 1999, Planet. Space Sci., 47, 855
Enzian A., Klinger J., Schwehm G., Weissman P. R., 1999, Icarus, 138, 74
Espinasse S., Klinger J., Ritz C., Schmitt B., 1991, Icarus, 92, 350
Espinasse S., Coradini A., Capria M. T., Capaccioni F., Orosei R., Salomone M., Federico C., 1993, Planet. Space Sci., 41, 409
Klinger J., 1980, Sci, 209, 271
Lamy P., Toth I., Fernandez Y. R., Weaver H. A., 2004, in Festou M. C. et al., eds, Comets II. Univ. Arizona Press, Tucson
Lisse C. et al., 2005a, ApJL, in press
Lisse C., A'Hearn M. F., Farnham T., Groussin O., Meech K. J., Fink U., 2005b, Space Sci. Rev., submitted
Morbidelli A., 1999, Celest. Mech. Dyn. Astron., 72, 129
Mousis O., Gautier D., Bockelée-Morvan D., Robert F., Dubrulle B., Drouart A., 2000, Icarus, 148, 513
Orosei R., Capaccioni F., Capria M. T., Coradini A., Espinasse S., Federico C., Salomone M., Schwehm G. H., 1995, A&A, 301, 613
Orosei R., Capaccioni F., Capria M. T., Coradini A., Sanctis M .C. D., Federico C., Salomone M., Huot J.-P., 1999, Planet. Space Sci., 47, 839
Orosei R., Coradini A., de Sanctis M. C., Federico C., 2001, Adv. Space Res., 28, 1563
Prialnik D., 2002, Earth, Moon, Planets, 89, 27
Russel H. W., 1935, J. Am. Ceram. Soc., 18, 1
Schultz P. H., Anderson J. L. B., 2005, Lunar Planet. Sci. Conf., 36, 1926

This paper has been typeset from a TEX/LATEX file prepared by the author.